Table I. Energies[a] and Total Energies[b] of MNDO- and 6-31G*-Optimized Species

species (point group)[e]	MNDO[a]	6-31G*//6-31G*[b]	MP2/6-31G*[b]	MP2/6-31+G*[b]	ZPE[a,c]	NIMAG[d]
			Toluene Series			
toluene (C_s)	13.57	−269.740 16	−270.627 10	−270.642 44	85.91	(0)
toluene/LiH[f] (C_s)	5.70	−277.747 36	−278.656 78	−278.667 72	89.54	(0)
toluene/$LiCH_3$[f] (C_s)	−18.74	−316.780 26	−317.822 10	−317.838 17	109.18	(0)
1a (C_1)	13.13	−276.573 77	−277.477 41	−277.494 72	78.11	(0)
1b (C_s)	9.85	−276.567 31	−277.473 75	−277.491 78	78.59	(0)
1c (C_s)	16.80	−276.573 36	−277.476 88	−277.494 55	78.02	(1)
1d (C_s)	*g*	−276.559 94	−277.470 28	−277.489 00	77.69	(1)
5a (C_{2v})	18.47	−269.078 53	*h*	*h*	75.25	(0)
7 (C_s)	8.43	−276.566 95	−277.468 70	−277.486 57	78.28	(0)
TS-α/LiH (C_s)	43.11	−277.675 61	−278.605 66	−278.621 33	86.56	(1)
TS-α/$LiCH_3$ (C_s)	29.79	−316.712 89	−317.774 59	−317.792 45	106.32	(1)
TS-*ortho*/LiH (C_1)	42.02	−277.663 32	−278.590 02	−278.607 25	86.78	(1)
TS-*ortho*/$LiCH_3$ (C_1)	28.92	−316.703 39	−317.761 48	−317.780 98	106.36	(1)
			Picoline Series			
4-picoline (C_s)	20.86	−285.734 74	−286.652 07	−286.668 96	78.26	(0)
5b (C_{2v})	16.93	−285.098 17		−286.064 41	68.63	(0)
6a (C_1)	18.66	−292.575 64	−293.508 19	−293.527 12	70.62	(0)
6b (C_s)	23.93	−292.573 76	−293.509 63	−293.528 29	71.35	(0)
6c (C_s)	22.33	−292.574 79	−293.507 81	−293.527 11	70.47	(1)
6da (C_{2v})[i]	35.11	−292.567 54	−293.495 93	−293.519 04	71.02	(0)
6e	*g*	−292.565 57	−293.502 26	−293.522 43	70.47	(1)
8 (C_{2v})	−11.99	−355.712 46		−356.852 224	89.42	(0)
LiH ($C_{\infty v}$)	23.21	−7.980 87	−7.995 96	−7.996 15	2.04	(0)
$LiCH_3$ (C_{3v})	−1.38	−47.015 54	−47.162 01	−47.166 64	22.28	(0)
H_2 ($D_{\infty h}$)	0.72	−1.126 83	−1.144 10	−1.144 10	6.64	(0)
CH_4 (T_d)	−11.95	−40.195 17	−40.332 44	−40.333 94	29.99	(0)

[a] Energies in kcal mol^{-1}. [b] Total energies in au (= 627.472 37 kcal mol^{-1}). [c] Zero point energy (*ab initio* calculations). [d] Number of imaginary frequencies (*ab initio* calculations). [e] Point group (*ab initio* calculations). [f] See Chart II. [g] Not a minimum or transition state. [h] **5a**. 6-31+G*//6-31+G*: −269.106 16. [i] **6da**. 6-31+G*//6-31+G*: −292.581 70 au.

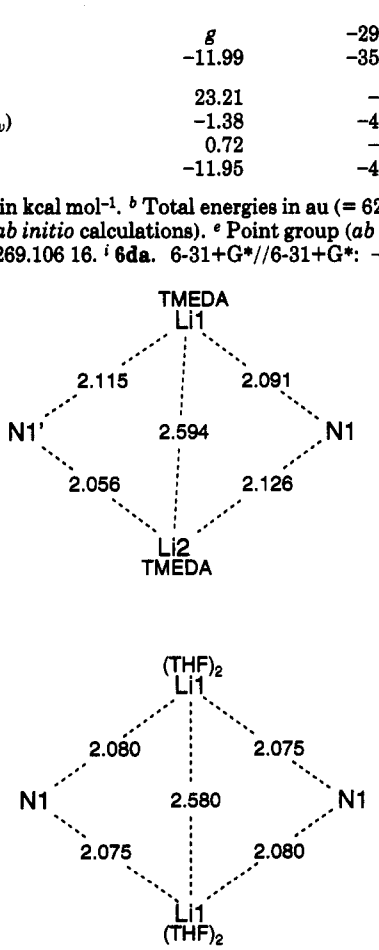

Figure 2. Central Li–N–Li–N segments of **4a** (TMEDA complex, top), and **4b** (THF complex bottom). Distances in Å.

geometries using the 6-31G* and 6-31+G* basis sets. Zero-point energies were scaled by 0.91.[11h] Atomic charges and bond orders were calculated using the natural population analysis (NPA) and natural bond orbital analysis (NBO) methods.[11i]

Lithiated 4-Picoline. Compared with 4-picoline, the 6-31+G* calculated structure of the corresponding C(α)-picolyl anion (**5b**) shows the expected changes resulting from its cross-conjugated π-system. These changes are most evident for the C(4)–C(α) and the adjacent C(3)–C(4) bonds. The former is converted to a typical C–C double bond (1.370 Å), and the latter is significantly elongated (from 1.388 to 1.448 Å). The C–C double bond character for the C(2)–C(3) bond increases. A slight lengthening results for the N(1)–C(2) bond (Table II). We use these values to quantify the influence of the lithium gegenion in the structures **6**. Diffuse functions do not change the geometries significnatly.[12] Therefore, for further discussions the 6-31G* results are used. For this pair of molecules, MNDO calculations reveal the same trends for bond length changes.

Three coordination modes of the lithium cation to the picolyl anion **5a** are conceivable (Chart II): benzylic lithiation (**6a**, η^3, and **6c**, η^2), ring lithiation (**6b**, η^5), and lithiation at nitrogen (**6da**). Structure **6e**, η^3, is the transition structure between **6a**/**6c** and **6b**. The geometries were calculated using the 3-21G and 6-31G* basis sets. In addition, **6da** was optimized on the 6-31+G* level. The results again indicate that diffuse functions have a minor effect on the geometry, but that the 3-21G calculated Li–N(1) bond is calculated to be too short (1.784 Å, compared with 1.819 (6-31G*) or 1.808 Å (6-31+G*)). Similar deficiencies of the 3-21G basis are observed for some of the C–Li distances of compounds **6a-c**. Some MNDO calculated bond lengths and further geometric parameters partly differ significantly from the *ab initio* results. The most significant difference was observed for the N(1)–Li distance in **6b** (MNDO, 2.408; 6-31G*, 2.036 Å).

(12) Kaufmann, E.; Tidor, B.; Schleyer, P. v. R. *J. Comput. Chem.* **1986**, *7*, 334.

Table II. Specific Bond Lengths (Å) of 6-31G*- and MNDO[a]-Optimized Species

species	X(1)–C(2)	C(2)–C(3)	C(3)–C(4)	C(4)–C(α)	Li–X(1)	Li–C(2)	Li–C(3)	Li–C(4)	Li–C(α)
				Toluene Series					
toluene	1.385	1.385	1.390	1.512					
	[1.405]	[1.406]	[1.414]	[1.505]					
toluene/LiH	1.390	1.390	1.395	1.511	2.565	2.573	2.598	2.629	
	[1.424]	[1.424]	[1.434]	[1.513]	[2.400]	[2.397]	[2.404]	[2.432]	
toluene/$LiCH_3$	1.389	1.390	1.395	1.510	2.599	2.600	2.612	2.639	
	[1.424]	[1.424]	[1.433]	[1.513]	[2.404]	[2.402]	[2.410]	[2.434]	
1a[b]	1.377	1.395	1.415	1.454			2.428	2.171	2.025
	[1.400]	[1.414]	[1.446]	[1.495]			[2.326]	[2.231]	[1.890]
1b	1.415	1.372	1.471	1.342	2.131	2.189	2.294	2.525	
	[1.446]	[1.406]	[1.498]	[1.361]	[2.172]	[2.237]	[2.229]	[2.325]	
1c	1.387	1.385	1.414	1.462				2.194	2.018
	[1.406]	[1.404]	[1.434]	[1.498]				[2.214]	[1.873]
1d	1.402	1.377	1.444	1.384	2.716	2.598	2.304	2.033	
	[c]								
5a	1.400	1.369	1.448	1.371					
5a: 6-31+G*	1.402	1.373	1.445	1.382					
5a: MP2/6-31+G*	1.408	1.389	1.422	1.396					
	[1.411]	[1.386]	[1.458]	[1.372]					
7[d]	1.392	1.400	1.412	1.518			1.998	3.028	3.308
	[1.408]	[1.403]	[1.436]	[1.526]			[1.819]	[2.430]	[2.402]
TS-α/LiH	1.387	1.387	1.414	1.460				2.125	2.253
	[1.403]	[1.413]	[1.446]	[1.507]				[2.242]	[2.148]
TS-α/$LiCH_3$	1.387	1.387	1.409	1.477				2.152	2.243
	[1.403]	[1.412]	[1.445]	[1.509]				[2.261]	[2.132]
TS-ortho/LiH	1.390	1.395	1.406	1.516			2.073		
	[1.409]	[1.405]	[1.436]	[1.529]			[2.039]	[2.403]	[2.349]
TS-ortho/$LiCH_3$	1.389	1.397	1.405	1.516			2.084		
	[1.408]	[1.406]	[1.437]	[1.529]			[2.033]	[2.440]	[2.362]
				Picoline Series					
4-picoline	1.321	1.384	1.388	1.509					
	[1.352]	[1.411]	[1.412]	[1.505]					
5b	1.341	1.362	1.450	1.360					
5b: 6-31+G*	1.341	1.366	1.448	1.370					
	[1.364]	[1.386]	[1.458]	[1.369]					
6a[e]	1.313	1.391	1.424	1.421			2.337	2.144	2.073
	[1.347]	[1.417]	[1.449]	[1.481]			[2.323]	[2.228]	[1.908]
6b	1.359	1.363	1.470	1.337	2.036	2.151	2.379	2.638	
	[1.382]	[1.411]	[1.497]	[1.359]	[2.408]	[2.325]	[2.204]	[2.299]	
6c	1.326	1.379	1.421	1.431				2.157	2.063
	[1.355]	[1.407]	[1.433]	[1.487]				[2.258]	[1.879]
6da[f]	1.373	1.339	1.463	1.336	1.819				
6da: 6-31+G*	1.372	1.344	1.462	1.343	1.808				
	[1.397]	[1.369]	[1.471]	[1.356]	[1.845]	[2.549]			
6db	1.371	1.341	1.465	1.339	1.819				
	[1.390]	[1.370]	[1.471]	[1.365]	[1.849]	[2.554]			
6db: X-ray[g]	1.375(8)	1.335(7)	1.455(8)	1.351(7)	2.090				
6dc	1.372	1.339	1.470	1.343	1.817				
	[1.389]	[1.371]	[1.370]	[1.378]	[1.853]	[2.570]			
6dc: X-ray[g]	1.375(7)	1.336(8)	1.449(8)	1.353(8)	2.097[i]				
6dc: X-ray[h]	1.376(7)	1.354(9)	1.462(8)	1.362(8)	2.078[i]				
6e	1.340	1.372	1.457	1.361	2.747	2.573	2.274	2.070	
	[c]								
8	1.382	1.338	1.466	1.335	2.008				
	[1.400]	[1.369]	[1.472]	[1.355]	[2.102]				

[a] MNDO-values in brackets. [b] Further bond lengths of **1a** (6-31G*, [MNDO]): X(1)–C(6), 1.398, [1.412]; C(5)–C(6), 1.374, [1.398]; C(4)–C(5), 1.419, [1.431]. [c] See Table I, footnote *g*. [d] Further bond lengths of **7** (6-31G* [MNDO]): X(1)–C(6), 1.380, [1.405]; C(5)–C(6), 1.389, [1.405]; C(4)–C(5), 1.387, [1.412]. [e] Further bond lengths of **6a** (6-31G*, [MNDO]): X(1)–C(6), 1.340, [1.362]; C(5)–C(6), 1.367, [1.400]; C(4)–C(5), 1.426, [1.431]. [f] MNDO results for **6da**: These values represent the most stable planar C_s structure. The C_{2v} structure is 0.16 kcal mol^{-1} less stable. [g] Data for the dimeric TMEDA complexes **3** and **4a**, see ref 9. [h] Data for the dimeric THF complex **4b**, see Figure 1. [i] Averaged value of the four Li–N bond lengths in the central Li–N–Li–N segment of **3**, **4a**, and **4b**; compare to Figure 2. Details for **3**: Li(1)–N(1), 2.065(9); N(1)–Li(2), 2.100(9); Li(2)–N(1'), 2.096(9); N(1')–Li(1), 2.099(9).

MP2(fc)/6-31+G*//6-31G* single-point calculations, corrected for ZPE differences (Tables I and III) predict the η^2, η^3, and η^5 isomers to be almost (that is, within 0.13 kcal mol^{-1}) equal in energy. Remarkably, the η^2-structure **6c** (a transition structure!) is indicated to have the lowest energy.[13] The "amide-like" structure **6da** is 5.6 kcal mol^{-1} less stable. Further data in Table I again stress the importance of the inclusion of electron correlation (at least up to second-order Møller–Plesset perturbation theory) and of diffuse functions to predict reliable energy differences.[12]

MNDO calculations result in very unrealistic predictions of the relative stabilities of the four isomers. Due to the strong overestimation of the Li–C bond energy, the destabilization of **6da** is overemphasized by about 11–16 kcal mol^{-1}. For the "η" structures, MNDO calculations predict the η^5 to be a η^6 isomer which is 5.2 kcal mol^{-1} less

(13) See, e.g.: Koch, W.; Schleyer, P. v. R.; Buzek, P.; Liu, B. *Croatica Chim. Acta* **1992**, *65*, 655.

Chart II

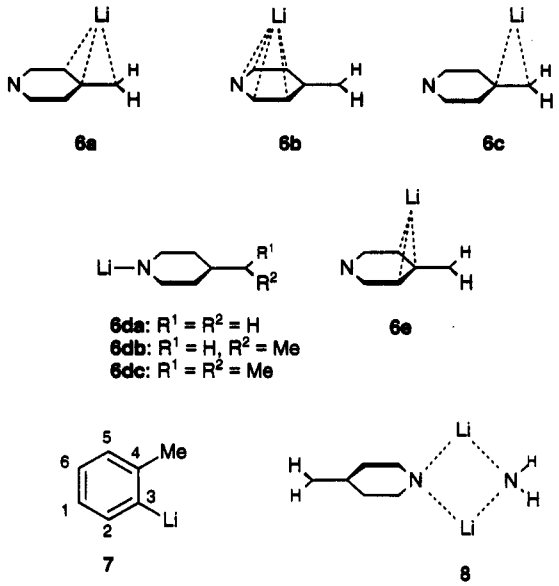

stable than the η^3 isomer. This does not agree with any of our *ab initio* calculations.

The anionic part of the ring lithiated isomer **6b** reveals the smallest differences compared with the free anion **5a**. The lithium cation prefers a coordination above the ring system near the nitrogen atom, which causes a relatively large Li–C(4) distance (2.638 Å). Therefore, this isomer has a η^5-structure while the analogous isomer in the benzyllithium series turns out to be "borderline" η^5/η^6 (see below). MNDO calculations underestimate this Li–N contact (6-31G*, 2.036 Å; MNDO, 2.408 Å) so that a η^6 structure results.

Changes in bond lengths are much more evident in the structures **6a** and **6c**. Both show a significant pyramidalization of the C(α) atom to which the lithium cation is predominantly coordinated. This parallels with the elongation of the C(4)–C(α) and C(3)–C(4) bonds, compared with **5b**. Furthermore, in the η^3 isomer **6a** the C(3)–C(4)–C(α)-Li subunit shows rough analogies to an unsymmetrical perturbed bridged allyllithium. Compared with the latter compound, the C(3)–C(4) and the C(4)–C(α) bonds are elongated (allyllithium, 1.392 Å;[3] **6a**, 1.424/1.421 Å). As expected, the degree of lithium coordination at the C(α) position parallels the elongation of the C(4)–C(α) bond lengths. This results in the ordering: **6da** (no coordination) < **6b** < **6e** < **6a** < **6c** (strongest coordination). These trends are predicted by MNDO calculations as well.

The most destabilized structure **6da** must be interpreted to be the parent compound of N(1)-lithiated 4-alkylidene-1,4-dihydropyridines. Its anionic moiety reveals only a very remote similarity with the anion **5b** or the η^5 structure **6b** (as reflected by the N(1)–C(2) and C(2)–C(3) bond lengths). Nevertheless, it compared quite well with our model for the "dimeric" gas-phase structure, **8**. N-Lithiation of **5b** causes a significant lengthening of the N(1)–C(2) bond (standard in **5b**: 1.341 Å), which is only expressed in **6da** (1.373 Å) and **8** (1.382 Å), but not in the more stable structures **6a** and **6c**. These trends are partly apparent from MNDO calculations. Apart from the obvious differences in the N(1)–Li bond lengths between **6da** and **8**, structure **6da** is the most simplified model to describe the structural properties of the heterocyclic moiety in such dimers adequately.

Finally, as a check of the above assumptions, we compare the characteristic X-ray data of **3**, **4a**, and **4b** with the calculated structures **6db**, **6dc**, and **8**: As summarized in Table II, the model compound **8** compares well with the essentials of the X-ray structure of the dimeric TMEDA complexes (**3** and **4a**) and the THF complex **4b** (Figure 1). Especially the 4-alkylidene-1,4-dihydropyridine moiety remains almost unaffected by TMEDA or THF complexation. This includes the averaged Li–N distances as well (**3**, 2.090 Å; **4a**, 2.097 Å; **4b**, 2.078 Å; compare **8**: Li–N(ring), 2.008 Å; Li–NH_2, 1.924 Å).

Ab initio calculations of such model "dimers" like **8**—which should include various substituents R^1 and R^2 (Chart II)—at any level of theory become rapidly prohibitive at present. Fortunately, the agreement between the N-lithiated structures **6bd** and **6dc** and the dihydropyridine moieties in **3**, **4a**, or **4b** is acceptable throughout and promising for future research.

Benzyllithium and *ortho*-Lithiotoluene. While lithiated picoline derivatives prefer bonding of lithium to the nitrogen (the least stable arrangement calculated for the isolated monomer, see above) in the solid state, theory[6,14] and experiment[15–18] agree on the general structure of benzyllithium. The first X-ray structure of benzyllithium, coordinated by two DABCO nitrogens,[15] shows attachment of the lithium cation to the benzylanion in a η^3 fashion. Lithium is mainly bound to C_α (the center of highest charge density, C–Li = 2.21 Å), but the C–Li bond is bent toward the aromatic ring (∠CCLi = 79.5°) and twisted 30° toward C_{ortho}, which results in contacts both to C_{ipso} (C–Li = 2.39 Å) and C_{ortho} (C–Li = 2.59 Å). The monomeric units are connected by bifunctional DABCO ligands to polymeric chains. A chain structure was also observed by Power *et al.*[16] for benzyllithium solvated with one molecule of diethyl ether. In this structure, each monosolvated lithium cation connects two benzyl anions. Lithium binds in a η^2 fashion to C_α and C_{ipso} of the anion (∠CCLi = 81.7°), while only one bond, to C_α, to the second anion is present. More recently, three crystal structures of benzyllithium and C_α-substituted derivatives, coordinated with TMEDA and/or THF, were published by Boche *et al.*[17,18] In these structures, the di- or tricoordinated lithium is located approximatly in the plane bisecting the benzyl moiety and is bound mainly to C_α. The C–C–Li angle varies from 76.9°, resulting in a η^2 structure, to 97.6°, which corresponds to a η^1-type structure.

The most stable structure calculated for the isolated benzyllithium monomer is the η^3 isomer **1a**.[6,14] **1c**(η^2) is the transition structure for the racemization of **1a** and corresponds to a very small barrier (0.03 kcal mol^{-1}, MP2/6-31G+G*//6-31G* + ΔZPE; a value of 0.25 kcal mol^{-1} was reported by Sygula and Rabideau[6]). A second minimum, **1b**, with the lithium cation bound in a η^5 fashion to the aromatic ring, is 2.28 kcal mol^{-1} less stable than **1a** (Sygula and Rabideau reported 1.69 kcal mol^{-1}). The barrier for interconversion between **1a**/**1c** and **1b**, via transition structure **1d**, is 3.21 kcal mol^{-1}. Thus, the

(14) Bühl, M.; v. Eikema Hommes, N. J. R.; Schleyer, P. v. R.; Fleischer, U.; Kutzelnigg, W. *J. Am. Chem. Soc.* **1991**, *113*, 2459.
(15) Patterman, P. S.; Karle, I. L.; Stucky, G. D. *J. Am. Chem. Soc.* **1970**, *95*, 1150.
(16) Beno, M. A.; Hope, H.; Olmstead, M. M.; Power, P. P. *Organometallics* **1985**, *4*, 2117.
(17) Zarges, W.; Marsch, M.; Harms, K.; Boche, G. *Chem. Ber.* **1989**, *122*, 2303.
(18) Zarges, W.; Marsch, M.; Harms, Koch, W. Frenking, G.; Boche, G. *Chem. Ber.* **1991**, *124*, 537.

Table III. Relative Energies[a]

compd	MNDO	6-31G*//6-31G*	MP2/6-31G*//6-31G*	MP2/6-31+G*//6-31G*	corr[b]
			Toluene Series		
1a	4.7	0.0	0.0	0.0	0.0
1b	1.5	4.05	2.30	1.84	2.28
1c	8.4	0.26	0.33	0.11	0.03
1d	-.-[c]	8.68	4.47	3.59	3.21
7	0.0	4.28	5.47	5.11	5.26
TS-α/LiH	1.1	0.0	0.0	0.0	0.0
TS-ortho/LiH	0.0	7.71	9.81	9.29	9.49
TS-α/LiCH$_3$	0.9	0.0	0.0	0.0	0.0
TS-*ortho*/LiCH$_3$	0.0	5.96	8.23	7.19	7.23
			Picoline Series		
6a	0.0	0.0	0.90	0.73	0.13
6b	5.2	1.18	0.0	0.0	0.06
6c	3.5	0.53	1.14	0.74	0.00
6da	26.4	5.08	8.60	5.80	5.56
6e	-.-[c]	6.32	4.62	3.68	2.93

[a] kcal mol^{-1}, based upon 6-31G* or MNDO geometries. [b] kcal mol^{-1}, including the ZPE correction. [c] See Table I, footnote *g*.

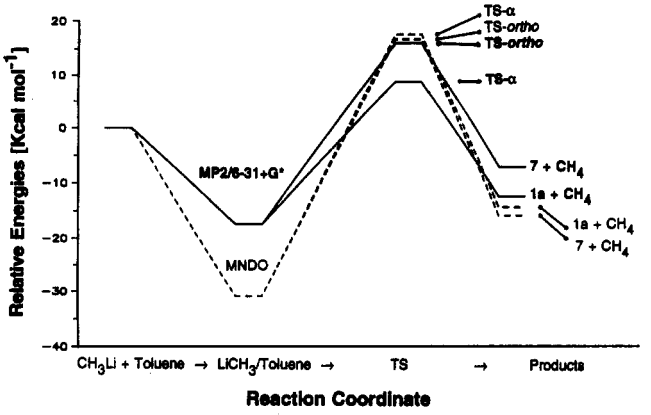

Figure 3. Energy profiles for benzylic and *ortho*-lithiation of toluene with CH$_3$Li (MP2/6-31+G*//6-31G* and MNDO results).

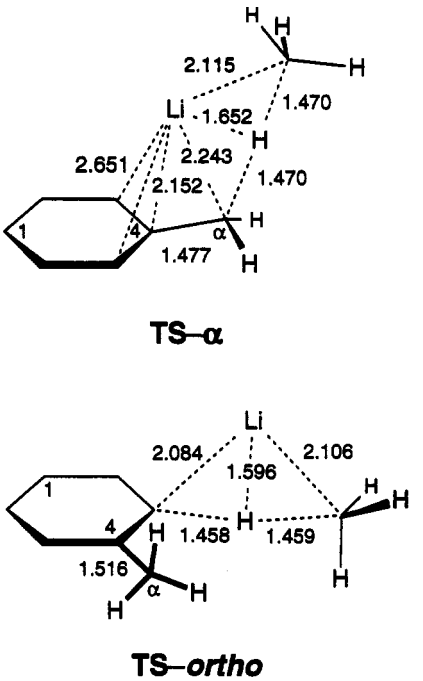

Figure 4. Transition structures for the benzylic (top) and *ortho*-lithiation (bottom) of toluene with CH$_3$Li (6-31G* results). Distances in Å.

potential energy surface for the movement of the lithium cation in benzyllithium is less flat than in the case of 4-picolyllithium. Nevertheless, the preference for **1a** over **1c**, i.e., to form an η^3 instead of an η^2 structure, is so small that the energy difference can easily be compensated by solvation and crystal packing effects.

The long C_{ipso}–C_{ortho} bonds (1.445 Å, 6-31+G*) and the short C_{ortho}–C_{meta} bonds (1.373 Å) are characteristic for the structure of the free benzyl anion. The C_{ipso}–Cα bond length is 1.382 Å. Furthermore, the *ipso* angle is significantly contracted, to 113.6°. Coordination of the lithium cation to the aromatic ring, giving the η^5 structure **1b**, leads to large changes in the geometry of the anion. The C_{ipso}–Cα bond is shortened by 0.1 to 1.342 Å, which approaches the length calculated for the C–C double bond, 1.317 Å.[19] The C_{ipso}–C_{ortho} bonds are strongly elongated, to 1.471 Å, and the *ipso* angle is contracted even further, to 112.3°. Changes in the opposite direction are seen when the lithium cation binds to Cα. The distances within the aromatic ring approach the values calculated for toluene (1.385-1.390 Å), while the C_{ipso}–Cα bond is elongated to 1.454 Å, in the η^3 structure **1a**, or to 1.462 Å in the η^2 structure **1c**. The bond lengths in the benzylic moiety of **1d**, the transition structure between **1a**/**1c** and **1b**, correspond almost exactly to the bond lengths of the free benzyl anion.

Due to the systematic overestimation of the C–Li bond energy by MNDO, the structures with *more* carbon lithium contacts are calculated to be too stable. **1b**, the η^5 structure, is found to be 3.2 kcal mol^{-1} more stable than the η^3 structure **1a**, while a value of 3.7 kcal mol^{-1} is computed for the racemization barrier via **1c**, which has only two carbon lithium contacts. An alternative C_7H_7Li isomer is *o*-lithiotoluene **7**, a species which is not observed in the metallation of toluene. However, MNDO calculations suggest that **7** is the most stable C_7H_7Li species.

In order to assess the reliability of the MNDO method in predicting the regioselectivity of aromatic metallations, we have included **7** in the present study and have calculated the activation barriers for the reaction of toluene and methyllithium (or lithium hydride) to yield benzyllithium and *o*-lithiotoluene, respectively (Figures 3 and 4). The results are summarized in Table III.

$$CH_3Li + \text{toluene} \rightarrow LiCH_3/\text{toluene (adduct)} \rightarrow \text{TS-}\alpha/LiCH_3 \text{ or TS-}o\text{-}LiCH_3 \rightarrow \mathbf{1a} \text{ or } \mathbf{7} + CH_4$$

The geometries obtained with MNDO show the same qualitative features as the 6-31G* optimized structures.

(19) The Carnegie Mellum Quantum Chemistry Archive, entry 4706.

Carbon–lithium distances are calculated to be too short with MNDO, due to the (well documented[20]) overestimation of the stability of the carbon lithium bond. Relative stabilities are calculated incorrectly. At all *ab initio* levels considered here, **7** is 4-5 kcal mol^{-1} destabilized relative to benzyllithium **1a**, which contrasts with the 4.7 kcal mol^{-1} *stabilization* computed with MNDO. Apparently, the overestimation of the carbon lithium bond strength by MNDO is more prominent when σ-type interactions are involved (in the case of **7**), than when the lithium interacts with a π-system, as in **1**.

These systematic errors also affect the energy profile calculated for the reaction between toluene and methyllithium. The strength of the initial complex, in which lithium is coordinated to the aromatic ring,[21] is grossly overestimated by MNDO, while the activation barrier for the *ortho*-lithiation is slightly lower (0.9 kcal mol^{-1}) than for the benzylic lithiation. Our *ab initio* results lead to the opposite conclusion: the barrier for the benzylic lithiation of toluene by methyllithium (8.7 kcal mol^{-1}, 25.1 kcal mol^{-1} relative to the initial complex) is 7.3 kcal mol^{-1} lower than for the *ortho*-lithiation (16 kcal mol^{-1}, 33.4 kcal mol^{-1} relative to the complex). Thus, the thermodynamic preference for benzylic metalation is accompanied by a clear kinetic preference for this reaction mode.

By means of MP2/6-31+G*//6-31G* *ab initio* calculations we have derived a model that predicts the degree of lithium coordination in the neighborhood of the Cα-center of benzyllithium or of lithiated 4-alkylpyridines. In both systems, the C_{ipso}–Cα (C(4)–C(α), Table II) bond length indicates the extent of interaction reliably. For lithiated 4-picoline, C_{ipso}–Cα varies between 1.336 Å for the C_{2v}-symmetrical N–Li structure **6da** (no coordination of Cα) and 1.431 Å for the strongest coordination (**6c**, η^2 at C4/Cα).

Though the potential energy surface for lithium cation movement is less flat, the same correlation was found for the comparable π-benzyllithium haptomers: The C_{ipso}–Cα bond length varies from 1.342 Å (**1b**, η^5 at both the C_{ortho}/C_{meta} centers and C_{para}; least expressed coordination) to 1.462 Å (**1c**, η^2 at C_{ipso}/Cα; strongest coordination). These results compare well with X-ray data published by Patterman *et al.*,[15] Power *et al.*,[16] and Boche *et al.*[17,18] X-ray investigations of dimeric TMEDA and THF complexes **3**, **4a**, and **4b** presented in this paper indicate that the structural parameters of the N-heteroaromatic ring systems (all N-substituted 4-alkylidene-1,4-dihydropyridines) agree surprisingly well with the most destabilized planar, "amide-like" N-lithiated C_{2v} or C_s symmetrical monomeric gas-phase structures, **6bd** and **6dc**. Thus, dimerization and the influence of donor coligands change the energetic ordering in the gas phase (preference for π-coordination) in favor of predominant N-lithiated structures.

While the relative energies of monomeric lithiated isomers **1a-d** and **6a-e** are calculated with MNDO reasonably well, some deficiencies of this method are evident. For benzyllithium/*o*-lithiotoluene (**1a-d**/**7**), MNDO does not describe the regioselectivity in competitive lithiations of alternative positions correctly. The semiempirical method favors *o*-lithiotoluene (**7**), whereas in *ab initio* calculations the benzyllithium isomers are more stable. The erroneous estimation of the relative activation barriers for the benzylic or *ortho*-lithiation of toluene is another example. The MNDO value appears to be too low and does not agree with any of our *ab initio* results. These lead to a clear preference for the benzylic lithiation.

Table IV. Energies, Relative to the Separated Reactants[a] (Toluene Series, 6-31G*-Optimized Geometries)

compd	MNDO	6-31G*	MP2/6-31G*	MP2/6-31+G*	corr[c]
toluene + LiH	0.0	0.0	0.0	0.0	0.0
toluene/LiH	−31.1	−16.52	−21.16	−18.28	−16.68
TS-α/LiH	6.3	28.50	10.92	10.83	9.57
TS-*ortho*/LiH	5.2	36.21	20.73	19.66	18.60
1a[b] + H_2	−22.9	12.82	0.97	−0.14	−2.91
7 + H_2	−27.6	17.10	6.44	4.97	2.21
toluene + $LiCH_3$	0.0	0.0	0.0	0.0	0.0
toluene/$LiCH_3$	−30.9	−15.41	−20.70	−18.25	−17.34
TS-α/$LiCH_3$	17.6	26.87	9.11	10.43	8.56
TS-*ortho*/$LiCH_3$	16.7	32.82	17.34	17.63	15.96
1a + CH_4	−11.0	−8.31	−13.01	−12.29	−12.37
7 + CH_4	−15.7	−4.03	−7.55	−7.17	−7.10

[a] kcal mol^{-1}. [b] MNDO: **1b** + H_2.

Experimental Section

Lithiated 4-Isopropylpyridine × 2THF, 4b. All reactions were carried out under an atmosphere of dry nitrogen. THF and benzene were freshly distilled from sodium; diisopropylamine and 4-isopropylpyridine were dried with KOH and distilled. NMR spectra (400 MHz for ^{1}H and 100.5 MHz for ^{13}C) were recorded on a JEOL JNM GX 400 FT spectrometer using Me_4Si as an internal standard.

A solution of 1.6 M n-BuLi in hexane (25 mL, 40 mmol) was added with a syringe to a solution of diisopropylamine (5.6 mL, 40 mmol) in THF at −10 °C. At this temperature and after the solution was stirred for 15 min, 4-isopropylpyridine (5.25 mL, 40 mmol) was added. After the solution was stirred for 1 h, the solvent was removed *in vacuo*. The residue was dissolved in THF (5 mL). **4b** was precipitated from this solution by addition of hexane (20 mL), filtered off, and washed with hexane (2 × 20 mL). A sample (2.0 g) of these yellow microcrystals was added to a mixture of benzene/THF (5:2, 10 mL), warmed to 60 °C, and then slowly cooled to room temperature to yield yellow crystal plates. ^{1}H NMR (THF-d_8): δ 6.36 (2 H, d, J = 7.3 Hz, H-2 and H-6), 5.12 (2 H, d, J = 7.3 Hz, H-3 and H-5), 1.40 (6 H, CH_3); ^{13}C NMR (THF-d_8) δ 142.5 (C-2, C-6), 133.0 (C-4), 105.2 (C-3), 78.0 (C-α), 19.5 (CH_3).

Crystal Data of 4b, [{4-(CH_3CCH_3)C_5H_4N}Li(THF)$_2$]$_2$: $C_{16}H_{28}Li_1N_1O_2$; M = 271.3; monoclinic system; space group $P2(1)/c$; a = 9.634(6) Å, b = 16.145(12) Å, c = 11.408(16) Å, β = 78.39(4); V = 1661(3) Å^3; Z = 4; D = 1.084 g cm^{-3}; $F(000)$ = 592; λ = 0.710 73 Å (Mo Kα); T = 200 K ± 1, graphite monochromator. Data were collected on a Nicolet R3m/V diffractometer using a crystal of dimensions 0.2 × 0.3 × 0.4 mm^3 by the ω scan method ($3.0° < 2\theta < 54.0°$). Three standard reflections were measured every 100 reflections. From 3658 unique measured data 1303 reflections with $F > 4.0\sigma(F)$ were used for structure solution (direct methods) and subsequent full-matrix least-squares refinement (SHELXTL Plus). All non-hydrogen atoms were refined anisotropically. The hydrogen atoms of the 4-isopropylpyridine were located by electron difference density map and were refined independent isotropically. The hydrogen atoms of the THF ligands were fixed in idealized positions using the riding model and were refined isotropically; 222 refined parameters; final R = 6.43%, final wR = 5.63%.[22]

Acknowledgment. E.A. gratefully acknowledges support by the Deutsche Forschungsgemeinschaft and the Fonds der Chemischem Industrie, and A.O. thanks the Universität Erlangen-Nürnberg for a scholarship. We thank Prof. Dr. P. v. R. Schleyer for useful discussions.

(20) Kaufmann, E.; Raghavachari, K.; Reed, A. E.; Schleyer, P. v. R. *Organometallics* **1988**, *7*, 1597.
(21) Kurz, S.; Hey-Hawkins, E. M. *Organometallics* **1992**, *11*, 2729.
(22) The author has deposited atomic coordinates for **4b** with the Cambridge Crystallographic Data Centre. The coordinates can be obtained, on request, from the Director, Cambridge Crystallographic Data Centre, 12 Union Road, Cambridge, CB2 1EZ, UK.

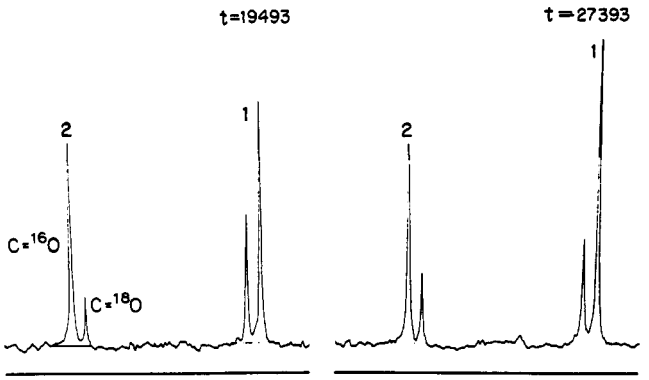

Figure 3. ^{13}C NMR spectra of 1 and 2 during $H_2{}^{18}O$ exchange at time t = 19493 s and 27393 s (the relative peak positions of C=^{18}O and C=^{16}O are indicated in the graph).

difference measurements.[23] Only those compounds with an axial sustituent gave an NOE between the proton geminal to the substituent and the ortho proton of the adjacent aromatic ring (see Table II, Experimental Section). For the determination of the effects of α substitution on rates, we have chosen to measure the rate of nucleophilic addition of $H_2{}^{18}O$ to the carbonyl of 1 relative to those of the α derivatives 2–12. For maximum accuracy, the relative rates were measured on solutions of pairs of ketones selected for their rate similarity in dioxane–water containing trifluoroacetic acid as a catalyst. The uptake of ^{18}O was monitored by ^{13}C NMR, making use of the isotope shift characteristic of the incorporation of ^{18}O into the carbonyl group of each ketone.[24] Figure 3 shows a typical example. As described in the Experimental Section, the peak-height ratios are treated by the method of Sachs[25] to obtain the rate constants for each spectral acquisition. Because of practical constraints associated with the NMR method, primarily the need for at least 128 transients over 4 min, for obtaining an adequate signal–noise ratio for the rapidly exchanged ketone, the rate constants are generally accurate to ±5%. Thus the spectra for run 1 (see Figure 3 and the Experimental Section) give the rate constants for 1 and 2 in Table I, from whose rate ratio $\Delta\Delta G^*$ or the difference in free energies of activation for the two exchange reactions is obtained (note that the absolute values of k_1 and k_2 are not significant, being dependent on the concentration of catalyst chosen for optimum initial rates). Also appearing in Table I are the relative rate data for the remaining derivatives, 3–12.

Results and Discussion

The Inductive Effect of the Substituent. A quantitative measure of the inductive effect is provided by the Taft substituent parameter σ^*. The value of σ^* for a methyl group is negligibly small (–0.1), but for a chloro or a methoxy group is substantial (1.05 and 0.52, respectively).[26] The influence of electronegative substituents on the hydration of simple carbonyl compounds is known to be appreciable. From a survey of the literature on the variation in K_d in simple α-halo and α-methyl derivatives of acetaldehyde and acetone, Bell[27] developed an empirical

Table I. Rate Measurements for Compounds 1–10

run	$k^a \times 10^4$	$k' \times 10^4$	rate ratio (k/k')	$\Delta\Delta G^*$, kcal/mol
1 (1 vs 2)	k = 0.55 (0.02, 5)	k = 0.11 (0.002, 4)	5.0	0.9
2 (1 vs 3)	k = 72.7 (0.8, 3)	k = 1.3 (0.03, 4)	56.0	2.3
3 (2 vs 3)	k = 10.7 (0.78, 3)	k = 1.0 (0.04, 5)	10.7	1.4
4 (3 vs 4)	k = 1.01 (0.03, 4)	k = 0.54 (0.02, 4)	1.9	0.4
5 (4 vs 5)	k = 0.84 (0.05, 4)	k = 0.049 (0.003, 4)	17.1	1.7
6 (1 vs 6)	k = 6.5 (0.3, 3)	k = 0.48 (0.015, 3)	13.5	1.5
7 (6 vs 7)	k = 2.10 (0.04, 4)	k = 0.230 (0.005, 4)	9.2	1.3
8 (7 vs 8)	k = 4.6 (0.2, 4)	k = 1.36 (0.02, 5)	3.4	0.72
9 (6 vs 9)	k = 2.11 (0.025, 3)	k = 0.70 (0.02, 4)	3.0	0.65
10 (8 vs 10)	k = 0.60 (0.01, 5)	k = 0.22 (0.01, 5)	2.8	0.60
11 (1 vs 11)	k = 8.9 (0.8, 5)	k = 1.7 (0.03, 4)	5.3	1.0
12 (1 vs 12)	k = 1.8 (0.03, 5)	k = 1.3 (0.02, 4)	1.3	0.15

From the data above, the following were obtained:

(1 vs 4)	2.7
(1 vs 5)	4.4
(1 vs 7)	2.8
(1 vs 8)	3.5
(1 vs 9)	2.15
(1 vs 10)	4.1

[a] For each reported rate constant, the average deviation and number of measurements are in parentheses.

equation, $\log K_d = 2.70 - 2.6\Sigma\sigma^* - 1.3\Sigma E_s$, where the dissociation constant for the diol was defined as K_d = [H_2O (mol fraction)][carbonyl compound]/[diol].[27] This equation thereby predicts more than a factor of 100-fold decrease in K_d per chloro substituent. Recognizing the possibility that the equation based on very small molecules might not be accurate when applied to larger ketones, we sought to examine the NMR spectrum of the dichloro ketone 8 for the presence of diol. In a 5% solution of water in dioxane-d_8, the spectrum of 8 showed a small singlet 0.03 ppm upfield of the singlet for the methyl group of 8. This singlet slowly increased, reaching its equilibrium concentration of 3.5% of methyl intensity of 8 after 2 days. Doubling the concentration of water increased the intensity ratio [diol]/[8], and the addition of a trace of trifluoroacetic acid (0.2%) accelerated equilibration. In this manner we have determined the value of K_d for 8, 6, and 1 to be 6, 9, and 9, respectively. Thus the effect of introducing one or two chlorine substituents on the stability of the diol intermediate is negligible. The effect of electronegativity of a chloro substituent on the transition state for isotopic change is more difficult to assess. The only previous pertinent study described the inductive effect of substituents in the mechanistically related reaction, the acid-catalyzed hydrolysis of a series of α-substituted acetone diethyl ketals.[28] In a dioxane–water mixture (1:1) the rate constants showed a very good Taft correlation[26] with σ^*, yielding a slope (ρ^*) of 3.5. Unfortunately, the value for ρ^* in the hydrolysis of ketals is not an appropriate model for predicting the slope of the Taft correlation for hydration

(23) Kotovych, G.; Aarts, G. H. M.; Bock, K. *Can. J. Chem.* **1980**, *58*, 1206–1210. Richarz, R.; Wüthrich, K. *J. Magn. Reson.* **1978**, *30*, 147–150.
(24) Risley, J. M.; Van Etten, R. L. *J. Am. Chem. Soc.* **1979**, *101*, 252–253. Vederas, J. C. *J. Am. Chem. Soc.* **1980**, *102*, 374–377.
(25) Sachs, W. H. *Acta. Chem. Scand.* **1971**, *25*, 3123–3134.
(26) Lowry, T. H.; Richardson, K. S. *Mechanism and Theory in Organic Chemistry*, 3rd ed.; Harper & Row: New York, 1987; p 153.
(27) Bell, R. P. *Adv. Phys. Org. Chem.* **1965**, *4*, 1–29.
(28) Kreevoy, M. M.; Taft, R. W., Jr. *J. Am. Chem. Soc.* **1955**, *77*, 5590–5595.

of derivatives of 1. The ketal hydrolyses can be expected to exhibit a larger slope for two reasons. First, the solvent polarity is much greater in the 50% aqueous mixture, as reflected in its much larger Y value.[29] Second, the ketal hydrolyses must involve a carbocation intermediate while the isotopic exchange is thought to proceed via the transition state 14, in which the positive charge is dispersed over an extra atom.[30] In the absence of a suitable model, we can use the equatorial derivatives of 1 to compare their relative rates from which both steric and inductive contributions can be assessed.

The Effect of Equatorial Substituents. An equatorial substituent will not be able to overlap with a nucleophile approaching the carbonyl since it is improperly aligned for any bonding interaction. In the absence of inductive effects, we can interpret any rate retardation as steric in origin. The slower exchange of 2 vs 1 is consistent with the development of two vicinal C/O interactions[31] during formation of the geminal diol intermediate[32,33] derived from 2. The observed retardation for 2 vs 1 (expressed as $\Delta\Delta G^{\ddagger}$) is found to be 0.9 kcal/mol. A comparison of the exchange of 5 vs 1 shows a much larger strain (4.4 kcal/mol) in the diequatorial transition state. This excess over additivity is surprisingly high and is the result of the unsymmetrical nature of the transition structure, as will be discussed later.

The increasing $\Delta\Delta G^{\ddagger}$ values for 2 (1.0), 11 (1.1), and 6 (1.5) more closely follow the order of increasing Taft E_s parameters for the methyl, methoxy, and chloro substituents, −0.07, −0.17, and −0.23, respectively, than that of their inductive substituent parameters, −0.1, 0.52, and 1.05. This indicates only a minor contribution from the inductive effect of these substituents.

The Effect of Axial Substituents. Table I shows that monoaxial methyl derivative 3 exchanges over 10 times more slowly than 2 and thus 56 times more slowly than 1. The rate for 3 reflects an increase in its free energy of activation ($\Delta\Delta G^{\ddagger}$) of 2.3 kcal/mol relative to that for 1. Let the effect of the axial substituent be represented by X as depicted in the free energy–reaction coordinate diagram shown in Figure 4. The free energy profile for 1 is symmetrical since the faces of its carbonyl are homotopic. For 3 the faces are diastereotopic; attack on either face by $H_2{}^{18}O$ will be retarded sterically, increasing the barrier. In addition, when attack occurs app to the methyl, there could be an electronic effect. One of the barriers will be increased (due to the destabilizing σ, $\sigma_{\ddagger}{}^{*}$ interaction of Cieplak) or decreased (due to the stabilizing $\sigma_{\ddagger}$, σ^{*} interaction of Anh). Naturally, both barriers must be traversed in an exchange, but only the higher one is measurable experimentally.

In the exchange of 4, symmetry is restored to the reaction coordinate as shown in Figure 4. The second methyl has to take the position which causes a smaller increase in activation barrier. Thus only a 0.4 kcal/mol increase in the free energy of activation is observed for 4 with respect to 3.

In an analogous fashion, the monoaxial chlorine in 7 causes a 2.8 kcal/mol increase in $\Delta G^{\ddagger}$, while the second axial chlorine raises the activation energy by an additional 0.7 kcal/mol. In dramatic contrast, the monoaxial methoxy

Table II. NOE Difference Measurements for 2–12

compd	proton irradiated	NOE[a]	compd	proton irradiated	NOE[a]
2	$-CHCH_3$	0	8	$-CHCl$	12
3	$-CHCH_3$	14	9	$-CHCl$	0
4	$-CHCH_3$	13	10	$-CHCl$ (axial)	16
5	$-CHCH_3$	0	11	$-CHOCH_3$	0
6	$-CHCl$	0	12	$-CHOCH_3$	13
7	$-CHCl$	14			

[a] Percent enhancement of the ortho proton of benzene ring.

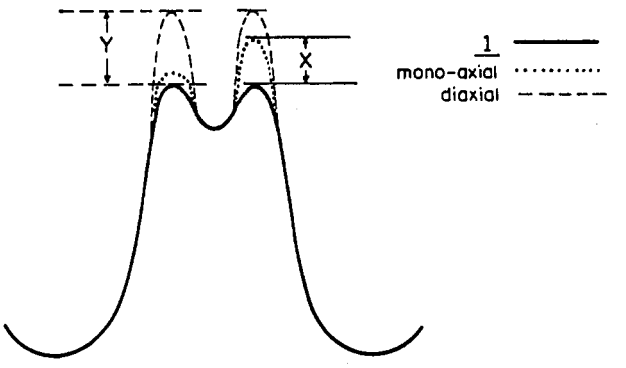

Figure 4. Free energy–reaction coordinate diagrams representing the isotopic exchange of 1, 3, and 4.

(29) Reference 26, p 339.
(30) Reference 26, p 667.
(31) To estimate the strain in the transition state for the reaction of 2 versus 1, we can use the Taft steric parameter E_s. E_s is defined as the log of the rate ratio (k_x/k_o) for the acid-catalysed hydrolysis of a substituted versus unsubstituted ethyl acetate,[22] thereby representing the substituent effect on the free energy of activation ($\Delta\Delta G^{\ddagger} = 2.3RT \log (k_x/k_o)$ for the transition state shown in formula 13. The major difference between 13 and that for isotopic exchange, 14, is the presence of two larger benzylic groups in 14. This could increase the steric factor over that (0.1 kcal/mol) derived from the E_s value of −0.07 for the methyl group.

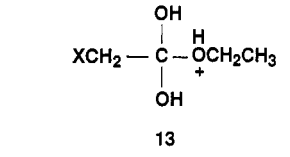

13

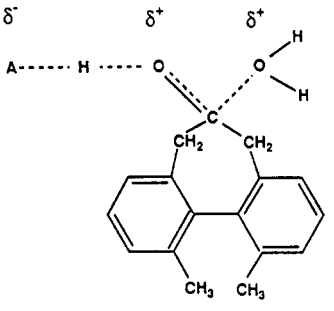

14

(32) For details on the mechanism of carbonyl hydration, see: Williams, I. H.; Spangler, D.; Femec, D. A.; Maggiora, G. M.; Schowen, R. L. *J. Am. Chem. Soc.* **1980**, *102*, 6619–6621. William, I. H.; Maggiora, G. M.; Schowen, R. L. *J. Am. Chem. Soc.* **1980**, *102*, 7831–7839.
(33) The presence of the diol intermediate (DI) allows "internal return" to compete with its transformation to labeled product. As Figure 4 indicates, for the symmetrical ketones 1, 4, and 5, the rate constants for these two processes will be equal except for a small kinetic isotope effect.[34] Although only one-half of the DI is converted to product, the consequent retardation by "internal return" is counterbalanced by the fact that the steady-state concentration of DI is doubled since it can be formed in two ways by attack of water on either equivalent face of the carbonyl. As a consequence, "internal return" in the exchange of a symmetrical ketone does not alter the Eyring relation between the observed rate constant k and the free energy of activation $\Delta G^{\ddagger}$.[35]
(34) Literature values for the $^{16}O/^{18}O$ kinetic isotope effect in the acid-catalyzed hydrolysis of several glucopyranosides have an average of 1.03 ± 0.005: Shiner, V. J., Jr.; Wilgis, F. P. In *Isotopes in Organic Chemistry*; Buncel, E.; Saunders, W. H., Jr., Eds.; Elsevier: Amsterdam, 1992; Vol. 8, p 302. This kinetic isotope effect will have no influence on the relative rates reported herein since its contribution will be the same for all exchange reactions.
(35) For a discussion of the effects of symmetry on rate constants, see: Laidler, K. J. *Chemical Kinetics*, 3rd ed.; Harper and Row: New York, 1987; p 100, 118.